This is the pre-peer reviewed version of the following article:
Soares-Silva, I., Sá-Pessoa, J., Myrianthopoulos, V., Mikros, E., Casal, M. and Diallinas, G. (2011), A substrate translocation trajectory in a cytoplasm-facing topological model of the monocarboxylate/H+ symporter Jen1p. Molecular Microbiology, 81: 805–817. doi: 10.1111/j.1365-2958.2011.07729.x**,**
which has been published in final form at
http://onlinelibrary.wiley.com/doi/10.1111/j.1365-2958.2011.07729.x/abstract.

A substrate translocation trajectory in a cytoplasm-facing topological model of the monocarboxylate/H^+ symporter Jen1p

Isabel Soares-Silva[a,2,3], Joana Sá-Pessoa[a,2], Vassilios Myrianthopoulos[b], Emmanuel Mikros[b], Margarida Casal[a,1] and George Diallinas[c,1]

[a]Centre of Molecular and Environmental Biology (CBMA), Department of Biology, University of Minho, Campus de Gualtar, Braga, 4710-057, Portugal

[b]School of Pharmacy, University of Athens, Panepistimiopolis, Athens 15771, Greece

[c]Faculty of Biology, Department of Botany, University of Athens, Panepistimioupolis, Athens 15781, Greece

[1]Corresponding authors: e-mail: mcasal@bio.uminho.pt or diallina@biol.uoa.gr

[2]Both authors contributed equally to the work

[3]Current address: Nephrology Research and Development Unit, Faculty of Medicine, University of Porto, Alameda Prof. Hernâni Monteiro, Porto, Portugal.

Keywords: structure-function relationships, lactate permease, specificity, molecular simulations, substrate docking

Summary

Previous mutational analysis of Jen1p, a *Saccharomyces cerevisiae* monocarboxylate/H^+ symporter of the Major Facilitator Superfamily, has suggested that the consensus sequence ^{379}NXX[S/T]HX[S/T]QD^{387} in transmembrane segment VII (TMS-VII) is part of the substrate translocation pathway. Here, we rationally design, analyse and show that several novel mutations in TMS-V and TMS-XI directly modify Jen1p function. Among the residues studied, F270 (TMS-V) and Q498 (TMS-XI) are critical specificity determinants for the distinction of mono- from di-carboxylates, and N501 (TMS-XI) is a critical residue for function. Using a model created on the basis of Jen1p similarity with the GlpT permease, we show that all polar residues critical for function within TMS-VII and TMS-XI (N379, H383, D387, Q498, N501) are perfectly aligned in an imaginary axis that lies parallel to a protein pore. This model and subsequent mutational analysis further reveal that an additional polar residue facing the pore, R188 (TMS-II), is irreplaceable for function. Our model also justifies the role of F270 and Q498 in substrate specificity. Finally, docking approaches reveal a 'trajectory-like' substrate displacement within the Jen1p pore, where R188 plays a major dynamic role mediating the orderly relocation of the substrate by subsequent H-bond interactions involving itself and residues H383, N501 and Q498.

Introduction

The transport of monocarboxylates, such as lactate, pyruvate and acetate, is essential for the metabolism and homeostasis of most cells. A family of monocarboxylate transporters (MCTs) has been reported that includes mainly mammalian members, which seem to be implicated in leukocyte-mediated immunity, hypoxia induced cellular responses, tissue partitioning of energy supply and tumor suppression (Ganapathy *et al.*, 2008; Merezhinskaya *et al.*, 2009). In fungi, activities for monocarboxylate-proton symporters have been found and shown to belong to two evolutionary distinct families. In *Saccharomyces cerevisiae,* one is encoded by the *JEN1* gene (Casal *et al.*, 1999) and another by the *ADY2* gene (Paiva *et al.*, 2004). These permeases exhibit differences in their mechanisms of regulation and specificity. Jen1p is a lactate-pyruvate-acetate-propionate transporter induced in lactic or pyruvic

acid-grown cells, whereas Ady2p, which recognizes acetate, propionate or formate, is present in cells grown in non-fermentable carbon sources (Casal *et al.*, 2008). Interestingly, Jen1p also transports selenite in a proton-dependent manner, which resembles the transport mechanism for lactate or pyruvate (McDermott *et al.*, 2010).

Jen1p, which is the only *S. cerevisiae* member of the Sialate:H^+ Symporter (SHS) Family (2.A.1.12) belonging to the Major Facilitator Superfamily (see below), has been extensively studied. It was the first permease of *S. cerevisiae* characterized by heterologous expression in *Pichia pastoris* at both the cell and the membrane vesicle levels (Soares-Silva *et al.*, 2003). The addition of glucose to lactic acid-grown cells very rapidly triggers loss of Jen1p activity and repression of *JEN1* gene expression (Andrade *et al.*, 2005). Jen1p activity is rapidly lost due to vacuolar degradation by endocytic internalization and sorting of newly synthesized polypeptides from the *trans*-Golgi to the MVB pathway. For both down-regulation pathways, Jen1p needs to be modified by ubiquitination with ubiquitin-Lys^{63} linked chain(s), through the action of the HECT-ubiquitin ligase Rsp5. Casein kinase 1-dependent phosphorylation is also required for Jen1p endocytosis (Paiva *et al.*, 2009). An evolutionary analysis has shown that several Jen1p homologues exist in all kinds of fungi (Lodi *et al.*, 2007). In yeasts like *Kluyveromyces lactis* and *Candida albicans*, the existence of two phylogenetically related Sc*JEN1*-like transporters with different specificities, namely for monocarboxylate (Jen1p subfamily) and dicarboxylate (Jen2p subfamily), was clearly demonstrated (Casal *et al.*, 2008; Lodi *et al.*, 2004; Soares-Silva *et al.*, 2004; Vieira *et al.*, 2010).

The MFS, where Jen1 belongs, constitutes the largest known family of secondary transporter proteins (Law *et al*,. 2008). They are responsible for the ion-coupled transport of a wide range of substrates, from monoamines to sugars to peptides. X-ray crystallography studies solving the structures of a handful of MFS revealed that the 12 TMS are arranged into two domains of 6 TMS each, which are related by a 2-fold pseudo-symmetry with an axis that runs normal to the membrane and between the two halves. Lactose permease (LacY), a proton/sugar co-transporter, is the prototype of the MFS proteins, not only because it is among the first crystallized, but mainly because there is a plethora of genetic, biochemical and molecular data, which have been accumulated within the last 30 years, mostly through the excellent work or the group of R. Kaback. These data have validated the structural

model and have shed light on how this molecule works through an alternating-access transport mechanism (Kaback *et al.*, 2011).

Structure-function relationships in Jen1p have been approached by using a rational mutational analysis of conserved amino acid residues (Soares-Silva *et al.*, 2007). In particular, functional studies of mutants concerning the conserved sequence ^{379}**N**XX[S/T]**H**X[S/T]**QD**XXX**T**^{391}, located towards the periplasmic side of putative transmembrane segment seven (TMS-VII), led to the observation that residues N379, H383 or D387 are necessary for function and specificity, while Q386 is important for the kinetics of Jen1p-mediated transport. Furthermore, 3D *in silico* modelling by homology threading using the structure of LacY (Guan *et al.*, 2006), further suggested that the conserved motif analyzed could be part of the substrate translocation pathway of Jen1p (Soares-Silva *et al.*, 2007). In this work we identified novel residues critical for the function and specificity of Jen1p. Subsequently, using a novel refined model created on the basis of Jen1p similarity with GlpT permease, an antiporter of glycerol-3-phosphate/inorganic phosphate (P_i) (Huang et al., 2003), and independent substrate docking studies, we reveal a substrate translocation trajectory in the inward-facing conformation of Jen1p, consisting mostly of the polar residues genetically identified as important for function.

Results

Rationale of mutation design

A rational, rather than a systematic, mutagenesis approach for Jen1p was based on two criteria. First, identify Jen1p amino acids that correspond to residues shown by crystallographic and functional studies to be involved in substrate recognition in LacY and GlpT, the two MFS permeases which exhibit the highest similarity score with Jen1p in homology threading approaches (see below and Experimental procedures). Second, identify by primary amino acid sequence alignments, Jen1p residues conserved in monocarboxylate transporters, but replaced by another conserved residue in dicarboxylate transporters of the Jen2p subfamily. While in both LacY and GlpT, a number of residues from several TMS contribute to substrate and H^+ binding, two residues in each case have been proposed to play primary roles in direct interactions with substrates. These are R144 (TMS-V) and K358 (TMS-XI) in LacY (Guan *et al.*, 2006), and R45 (TMS-I) and R269 (TMS-VII)

in GlpT (Huang *et al.*, 2003). In Jen1p, these residues correspond to F270, N501, F156 and H383, respectively. We have previously analyzed mutations concerning H383 and have shown that this residue is absolutely essential for function (Soares-Silva *et al.*, 2007). In the present work, we undertook the analysis of F270, N501 and several of their neighboring residues. Our choice was further strengthened by the following observations.

F270 is a well conserved hydrophobic residue in monocarboxylate transporters (Phe or Leu), but is replaced by a conserved Gln in dicarboxylate transporters (Fig. 1). An evolutionary relationship of mono and di-carboxylate transporters was previously reported (Casal *et al*,, 2008). Based on α-helical wheel projection of TMS-V, we also noticed that on the same side of F270 lies an absolutely conserved Ser residue (S266) and three well conserved bulky aromatic amino acids (Y273, F277, Y284). Among the latter, Y284 is replaced by Gln in dicarboxylic acid transporters and Ala or Asn in other Jen1p homologues of unknown specificity. Furthermore, we noticed that on the opposite side of the TMS-V helix of Jen1p, A272 is conserved in monocarboxylic acid transporters, but is replaced by Gly in dicarboxylic acid-specific homologues (see Fig. 1). Finally, N501 and its neighboring Q498 are two absolutely conserved polar residues, present in the middle of TMS-XI of all Jen1p homologues, including mono- and di-carboxylate permeases (Fig. 1).

Based on the above observations we made the following 23 *JEN1* mutations: F270Q, F270L, F270A, F270P, F270G, F270Y, S271Q, S271E, F270Q/S271Q, F270Q/S271E, Y273A, Y284T, Y284A, Y284Q, S266T, S266A, A272G, Q498A, Q498N, Q498E, N501A, N501Q, N501D. All mutations were constructed on plasmid pDS-1, which contains the *JEN1* sequence under the control of the *GPD* promoter, and introduced through genetic transformation into a *S. cerevisiae jen1*Δ *ady2*Δ strain, based on *ura3*$^{-}$ complementation (Soares-Silva *et al.*, 2007). The recipient strain lacks carrier-mediated monocarboxylate transport activity and thus allows the direct assessment of plasmid-borne *JEN1* mutations.

Jen1p function and specificity is differentially affected in several mutants.

Fig. 2 shows a relative comparison of Jen1p-mediated [^{14}C]-lactic acid transport in control strains and mutants. Mutants could be classified into two basic types; a) those reducing or abolishing (≤ 30%) Jen1p-mediated transport (S266T, F270L, F270P,

F270Q, F270Q/S271E, Y273A, Q498E, N501Q, N501D, N501A), b) those affecting moderately (~60-210%) Jen1p-mediated transport (S266A, F270G, F270Y, F270A, S271Q, S271E, F270Q/S271Q, A272G, Y284Q, Y284T, Y284A, Q498N, Q498A). Our results showed that several specific substitutions of S266, F270, Y273 and Q498, and all substitutions of N501, behave as loss-of-function mutations. In order to test whether mutations affecting the apparent Jen1p activity do so due to a direct effect on transport, rather than an effect on Jen1p expression in the plasma membrane, we re-constructed several of these mutations in a fully functional GFP-tagged version of Jen1p (see Experimental procedures), giving particular priority to those negatively affecting Jen1p-mediated transport. Figure 3 shows that none of the mutations tested affects the expression of Jen1p in the plasma membrane of *S. cerevisiae*, strongly indicating that these mutations affect Jen1p transport function *per se.*

We tested the growth of control strains and mutants on monocarboxylates and dicarboxylates (succinic or malic acid) as sole carbon sources. In the conditions used (see Experimental procedures), *S. cerevisiae* does not possess detectable dicarboxylate transporter activities, so any mutation conferring to Jen1p the ability to take up dicarboxylates could be revealed by these growth tests. Figure 4A shows that all Jen1p mutants carrying alleles reducing Jen1p activity (< 33 %) led to practically no growth on lactic acid. Two exceptions concerned mutants S271Q and S271E, which do not grow on lactic acid media, although they are active (>60 %) for [^{14}C]-lactic acid transport. As growth tests were performed at 18 ^{o}C and uptakes at 30 ^{o}C, for technical reasons, we thought that this apparent discrepancy might be due to cryosensitivity of these mutants in respect to Jen1p function. We confirmed that this was indeed the case by performing uptake assays at lower temperatures (18 ^{o}C), which showed that both S271Q and S271E had very low Jen1p activity at this temperature (see Figure 2).

Most interestingly, specific mutants (F270G, F270A, F270Q/S271Q, Q498A) showed significant Jen1p-dependent growth on succinic acid. No mutant showed significant Jen1p-mediated growth on malic acid, but this might have been expected as *S. cerevisiae* has a low effectiveness of malate metabolism (Boles *et al.*, 1998). These results confirmed that N501 is a critical residue for function, whereas residues F270 and Q498 are critical for function, but mostly act as determinants of Jen1p specificity.

We finally tested the growth behaviour of all mutants described previously (Soares-Silva *et al.*, 2007) and herein in respect to their resistance/sensitivity to selenite (McDermott *et al.*, 2010). Figure 4B shows that, as expected, most loss-of-function mutants (transport activities < 65%) are relatively resistant to selenite, whereas fully active mutants (transport activities > 104%) are fully sensitive. However, there are three exceptions concerning mutants S271Q, Q498A and N379Q, in which lactate transport and selenite sensitivity were uncoupled. This observation is in line with a fine role of a relevant residue in determining Jen1p specificity (see later).

Specificity and kinetic profile of functional mutants

We estimated inhibition values for the uptake of radiolabelled lactate in the presence of non-radiolabelled lactic, pyruvic, succinic and malic acids (Table 1). The inhibitors were supplied at concentrations close to previously established $K_{m/i}$ values for lactic (0.3 mM) and pyruvic (0.7 mM) acid, or at 60 mM for the non-physiological substrates, succinic and malic acid. In these conditions, the control strain expressing wild-type Jen1p conserves 30-40% [^{14}C]-lactic acid transport activity in the presence of unlabelled lactic or pyruvic acids and 100% activity in the presence of either succinic or malic acids. Most functional mutants (≥ 20% Jen1p transport activity) conserve a wild-type specificity profile with a practically unchanged capacity for lactate or pyruvate binding, and an inability to bind succinate or malate. However, five mutants showed a significantly different profile. In A272G, Jen1p seems to be more efficiently inhibited by unlabelled lactic and pyruvic acid. In contrast, in N501D, Jen1p activity is much less efficiently inhibited by unlabelled lactic or pyruvic acid. These results suggested (and subsequently shown) that A272G and N501D have increased and reduced affinity for lactate, respectively. Three other mutants, F270G, F270A and F270Q/S271Q, showed an increase in their binding affinity for succinic or malic acids. In these mutants, the remaining activity for radiolabelled lactic acid transport in the presence of succinic or malic acids ranged from 24-50%, compared to 62-104% in the wild-type and other mutants. In mutant Q498A, which could only grow weakly on succinic acid (see Fig. 4A), we did not detect any measurable competitive effect of dicarboxylic acids on [^{14}C]-lactic acid transport.

K_m and V_m values for lactate transporter were determined in selected mutants, namely S266A, F270G, F270Q/S271Q, A272G, Q498A and N501D (Table 2). As expected, mutations Q498A and N501D led to reduced affinity for lactate (~2.5-fold increase in K_m values compared to wild-type), whereas F270Q/S271Q and A272G led to increased affinity for lactate (3.5-fold reduction in K_m values). V_m values were little affected (~0.5-fold increased or reduced) in all mutants analyzed. K_i values for succinic and malic acids were also estimated in F270G, F270Q/S271Q and Q498A (Table 3). The first two mutants had acquired relatively high affinities for succinic acid binding (<2 mM), whereas Q498 showed measurable but low affinity (30 mM) for this acid. Finally, although all three mutants had measurable affinities for malic acid, only F270G had relatively high affinity for this substrate. These results showed that Jen1p mutants F270G, F270A and F270Q/S271Q and Q498A recognize and transport dicarboxylates.

A structural model for Jen1p and prediction of a major functional role of R188

Molecular simulations were undertaken in order to build a Jen1p model on the basis of its sequence similarity with four different MFS proteins of known crystallographic structure, namely GlpT (Glycerol transporter of *E. coli* (Huang *et al.*, 2003), LacY (Lactose permease of *E. coli* (Guan *et al.*, 2006), FucP (Fucose Transporter of *E. coli* (Dang *et al.*, 2010)) and PepT (Oligopeptide of *Shewanella oneidensis* (Newstead *et al.*, 2011)). LacY, FucP and PepT are bacterial proton symporters, whereas GlpT functions as an inorganic phosphate antiporter. Among them, the first three correspond to an inward-facing conformation, occluded from the periplasmic side of the membrane, whereas the FucP is the only MFS member captured in an outward-facing conformation. The best model was obtained on the GlpT structure (for details see Experimental procedures). The overall topology of the modeled Jen1p (Fig. 5) was in good agreement with all the structures of other MFS members.

In the modeled Jen1 structure (Fig. 5), the occurrence of polar residues within the core helical domains was, as might be expected, markedly low, with the exception of residues annotated as critical for function (N379, H383, Q386, D387, Q498 and N501), plus a fully conserved Arg residue (R188) located within TMS-II (Fig. 1). We mutated R188 (R188A and R188K) and found that substitution of R188 does not affect the plasma membrane expression of Jen1 (see Fig. 3), but abolishes Jen1p transport activity (see Fig. 2 and 4). Thus, R188 proved to be a novel residue

absolutely essential for Jen1p function. The importance of this residue is further discussed later. Almost all acidic and basic residues were located mostly at the two termini and in interhelical or interdomain flexible regions of the protein, where they appeared as engaged in salt-bridging pairs. Notably, the occurrence of polar residues in transmembrane domains was mostly limited to helices VII and XI, with the exception of R188 belonging to TMS-II. Most interestingly, the side-chains of all polar residues faced the protein pore and formed an extended network of hydrogen bonds along the entire open pore cavity (Fig. 5). This network was located approximately at the central part of the pore, demonstrating a very characteristic, spiral rim-like arrangement. Furthermore, functionally essential polar residues (N379, H383, Q386, D387, Q498 and N501) were aligned in a row along an imaginary axis that lies parallel to the protein pore.

The phenyl side-chain of F270 (TMS-V) was in close proximity to helices VIII and X, forming extensive edge-to-face π-π stacking interactions with F470 and W473 (TMS-X), and was in close contact with surrounding aromatic residues (W149, Y246, F269 and F270), forming a wide network of local hydrophobic interactions. Notably, the phenyl ring of F270 showed an additional close contact with TMS-VIII and more particularly at the middle of the helix where a characteristic kink appears. On the other side, its adjacent residue S271 interacted in an intra-helical fashion with the backbone of G267 and also formed an interhelical interaction with the side-chain of Y146 (TMS-I) (Fig. 6). While the location of the pair F270-S271 along the pore axis could account for their role as substrate specificity determinants, the aromatic ring of F270 could also facilitate helix packing and consequently enhance tertiary structure stabilization.

Molecular simulations of substrate-transporter recognition

Jen1p-substrate recognition was addressed by docking calculations. The simulation of the complex of Jen1p and lactate resulted in an unambiguous "trajectory-like" displacement of the monocarboxylate within the pore (Fig. 7 and 8). The starting point of this trajectory was in close proximity to the periplasmic side while the ending point was in the depth of the pore, towards its cytoplasmic opening. The substrate translocation course was almost parallel to the transporter axis and sequentially engaged a number of attractive hydrogen bonding interactions originating from residues H383, R188, N501 and Q498. The translocation of the substrate was

accompanied by a conjugated reorientation of the side-chains of the aforementioned residues. In such a mode, the collective conformational change observed through calculations suggested an orderly relocation of the substrate over a hypothetical track defined by subsequent interactions formed between it and the side-chains of those four critical residues. Among them, the side-chain of R188 seemed to undergo the more pronounced rotameric transition. A 4.4Å shift of the guanidinium group was observed as accompanying the repositioning of lactate from the vicinity of H383 towards N501 and Q498 at the inward-facing exit of the pore (Fig. 5). Interestingly, when non-interacting with the substrate, the R188 guanidinium was stably anchored to those two specific side-chain amides by three hydrogen bonds (Fig. 7). In the majority, however, of docked poses the lactate molecule was fully hydrogen bonded to the corresponding residue pairs (R188-H383, R188-N501 and R188-Q498) along the course of the translocation. Due to its inherent flexibility, the side-chain of R188 could be considered as a key residue in a mechanistic interpretation of the translocation process. Additionally the loss of R188 side-chain flexibility in the Q498E mutant due to the expected formation of a salt bridge between R188 guanidinium and E498 carboxylate could explain the observed loss of function of this mutant, further illustrating R188 critical role.

In contrast to results derived from docking calculations of the Jen1p-lactate complex, simulating the recognition of a dicarboxylic species (succinate) by the transporter afforded no acceptable docked poses, with this outcome being in agreement with experimental data. On the other hand, the simulation of F270G or the doubly mutated F270Q/S271Q Jen1p versions in association with succinate, did afford several docked poses resembling the wild-type transporter-lactate recognition and translocation track. This was in line with the fact that these mutants exhibited relatively high affinities for this dicarboxylic acid (Table 3). Finally, simulation of the Q498A mutant, which had very low affinity for succinic acid (Table 3), did not show any docked pose for this substrate.

Discussion

We have mutated several residues in TMS-V and TMS-XI of Jen1p, based on the rationale that their location might be analogous to that of residues known to be involved in substrate binding in MFS permeases or the observation that they are

differentially conserved in mono- and dicarboxylate transporters. Functional analysis of the mutants showed that N501 is critical for physiological function (all relevant substitutions led to < 30% activity), whereas F270 and Q498 are critical for transport kinetics and for restricting Jen1p specificity to monocarboxylates. Several other residues (S266, S271, A272, Y273) in the vicinity of F270 were also shown to be relatively important for the transport characteristics of Jen1p. In a previous mutational analysis, we have shown that residues N379, H383 and D387, in TMS-VII, are irreplaceable for function, whereas Q386 affects the kinetics of Jen1p-mediated transport.

Using a novel refined model created on the basis of Jen1p similarity with GlpT permease, we subsequently located the relative position of all functional residues, as identified by mutational analysis, within the 3D structure of Jen1p. All critical polar residues were thus shown to be perfectly aligned in a row (in the order D387, H383, N379, N501, Q498) along an imaginary axis that lies parallel to a protein pore, which is occluded towards the periplasmic side and open towards the cytoplasm. Most importantly, the model predicted a major functional role of another polar residue facing the pore, namely R188. Mutational analysis of this residue confirmed this prediction and further validates the model. The 3D model built also predicts that the location of F270 and Q498 could justify their role in substrate specificity. More specifically, the proximity of the phenyl ring to the kink of TMS-VIII might seriously influence the dynamic behavior of the transporter during the transition between the inward and outward conformations. This is consistent with mutational analysis showing that replacement of phenylalanine by residues of the same bulk that lack aromaticity (F270P, F270L, F270Q) impaired Jen1p function, whereas substitutions with more flexible or polar residues (F270A, F270G or F270Q/S271Q) facilitated the recognition and accommodation of dicarboxylates. What is also noticeable is that F270 and Q498 are positioned at the same level towards the opening of the inward-facing pore, and thus could act as gating element or filters which restrict the translocation of substrates other than monocarboxylates. Similar inward-facing selectivity elements have been recently described in the UapA transporter of *Aspergillus nidulans* (Kosti *et al.,* 2010).

Independent substrate docking approaches revealed a putative ‘trajectory-like’ displacement of the substrate within the Jen1p pore. The major residues involved in

this trajectory were H383, N501, Q498 and R188. In this trajectory, the Arg residue seems to play a dynamic role by mediating the orderly translocation of the substrate through subsequent H-bond interactions involving itself and residues H383, N501 and Q498. This idea is in line with the observation that R188 mutations impair Jen1p. In GlpT, two conserved arginine residues, R45 from TM-I and R269 from TM-VII, are located at the inner end of the substrate-translocation pore of the GlpT structure, strategically placed to interact directly with substrate as central components of the binding site (Huang *et al.*, 2003). Noticeably, R269 of GlpT corresponds to H383 in Jen1p, in line with the observation that basic residues are often essential for function in MFS transporters (Huang *et al.*, 2003). Two other residues that have been reported as critical for GlpT function, H165 and D274 (Huang *et al.*, 2003), correspond to functionally important residues in Jen1p: Y273 and D387, respectively.

Residues D387 and N379, which are elements of the "signature" motif located across the half-length of the pore, and which have been shown to be functionally irreplaceable (Soares-Silva *et al.*, 2007), did not form any direct interactions with the substrate. At least for D387, this should be expected since in the inward-facing modeled conformation of the transporter, this residue lays almost totally buried within the contracted periplasmic lobe of the protein. As the Jen1p model was built based on the inward-facing conformation of GlpT, the substrate trajectory defined does not mean to describe the entire trajectory that lactate follows in order to be translocated along the membrane axis. In agreement with the model proposed by Kaback and co-workers (Guan *et al.*, 2006; Mirza *et al.*, 2006), we speculate that upon binding of the substrate-proton pair at the end of a putative outward-facing trajectory, a major conformational change might be elicited to create the inward-facing trajectory. In this mechanism, substrate translocation might involve sliding between critical nodal points within the outward- and inward-facing alternating pores. This notion is supported by recent molecular dynamic approaches which showed that in a modeled outward-facing conformation of LacY, based on the outward-open conformation of FucP (Dang *et al.*, 2010), the substrate remains in the pocket but slides and binds with several different residues compared to the view obtained from the inward-facing structure (Newstead *et al.*, 2011). Interestingly, sequential binding sites and substrate sliding from one (external) to the other (internal) have been recently proposed in the

AdiC transporter (Kowalczyk *et al.*, 2011) and the GLUT MFS subfamily of hexose transporters (Cunningham *et al*., 2006; Manolescu *et al*., 2007; Naula *et al*., 2010).

Experimental procedures

Yeast strains and growth conditions. The *S. cerevisiae* strain W303-1A *jen1*Δ *ady2*Δ, lacking monocarboxylate uptake capacity, was used to express *JEN1* mutants from a low copy plasmid (pDS-1, see below). Cultures were maintained on slants of yeast extract (1%, w/v), peptone (1%, w/v), glucose (2%, w/v) and agar (2%, w/v) or minimal media with required supplements for growth. Yeast cells were grown in yeast nitrogen base (Difco), 0.67%, w/v (YNB medium), supplemented as required, or in yeast extract (1%, w/v), peptone (1%, w/v) (YP medium). Carbon sources were glucose (2%, w/v), lactic acid (0.5%, v/v, pH 5.0), pyruvic acid (0.5%, w/v, pH 5.0), succinic acid (1%, w/v, pH 5.0), malic acid (1% w/v, pH 5.0). Growth was carried out at 30 ºC. Cultures were always harvested during the exponential phase of growth. For derepression conditions glucose-grown cells were centrifuged, washed twice in ice-cold deionised water and cultivated into fresh YNB medium supplemented with lactic acid for 4 hours. For drop tests, cells were grown on YNB Glu-Ura media, until a OD_{640nm} of 0.1 was reached. A set of three 1:10 serial dilutions was performed and 3 μl of each suspension was inoculated in the desired medium, using YNB Glu-Ura as a control. Cells were incubated at 18ºC for 10 days or alternatively at 30ºC for 3 days. At 18 ^{o}C carboxylic acid uptake by diffusion is drastically reduced so that growth on lactic acid as sole carbon source is directly dependent on a functional Jen1p transporter. For selenite sensitivity tests, strains were grown on YNB-glucose medium supplemented with 200 μM sodium selenite.

Construction of *JEN1* mutations. Plasmid isolation from *E. coli* strains and DNA manipulations were performed by standard protocols. *JEN1* mutations were constructed in centromeric plasmids, under the control of the GPD promoter, pDS1 (WT-Jen1) or pDS1-GFP, the latter carrying a gfp-tagged version of *JEN1*, with oligonucleotide-directed mutagenesis as previously described (Soares-Silva *et al.*, 2007). The oligonucleotides used are listed in SI Table 1. Mutations were confirmed by sequencing. The mutant alleles were introduced in a *S. cerevisiae* W303-1A *jen1*Δ

*ady2*Δ strain, and transformants were selected on complementation of uracil auxotrophy. As a control the strain was also transformed with the original vector p416GPD.

Epifluorescent microscopy. Samples for fluorescence microscopy were grown, at 30 °C until midexponential growth phase and then shifted under derepressed conditions for Jen1p expression (YNB lactate 0.5% (v/v), pH 5.0) for 4 h (Soares-Silva *et al.*, 2007). Samples were at this point immobilized on coverslips using one volume of low-melting agarose and then directly observed on a Leica DM5000B epifluorescent microscope with appropriate filters. The resulting images were acquired with a Leica DFC 350FX R2 digital camera using the LAS AF V1.4.1 software. Images were then processed in the Adobe Photoshop CS2 V9.0.2 software.

Transport assays. Measurement of transport activity and competition assays were performed as previously described (Soares-Silva *et al.*, 2007) using radiolabelled D,L-[U-^{14}C] lactic acid (Amersham Biosciences).

Model construction, validation and molecular simulations. Sequence similarity was determined by a HMM-HMM comparison with HHpred software (http://toolkit.tuebingen.mpg.de/hhpred). The HMM profile query afforded four distinct structural templates from bacteria, the glycerol-3-phosphate transporter GlpT (pdb entry: 1PW4) (Huang *et al.*, 2003), the lactose permease LacY (pdb entry: 1PV7) (Abramson *et al.*, 2003), the fucose permease FucP (pdb entry:3O7Q) (Dang *et al.*, 2010) and the oligopeptide permease PepT (pdb entry:2XUT) (Newstead *et al.*, 2011). Alignments were created for all four templates and relevant models were built using MODELLER software (Sali *et al.*, 1995). A stepwise validation approach was followed, consisting of MD model optimization, comparison with existing experimental data and, finally, visual inspection. First, theoretical models were subjected to 2.5ns of Stochastic Dynamics simulation and found relatively stable, with a measured RMS deviation of alpha carbons from starting coordinates not exceeding 3Å. After SD optimization, the two best models, those built on GlpT and LacY, were tested for structural consistency by considering all available experimental data. Both were in good accordance with the proposed substrate translocation pathway as it was outlined by observations based on mutagenesis and kinetics studies presented

previously and in the present study. The constructed models were not of identical structural quality. Visual inspection has revealed a number of secondary structure inconsistencies on the homology-derived model built on LacY. A second issue regarding this particular model was the width of the protein pore. The LacY transporter facilitates the translocation of disaccharides, molecules that are far bulkier that the corresponding substrates of GlpT transporter. As a result, the pore of the two templates differs in width significantly. Given that the homology modeling protocol utilized herein does not allow for major conformational changes of the modeled proteins and induced fit, the pore width would be solely dependent on the template used. It was reasoned that the pronounced similarity of the physicochemical profile and steric volume between glycerol-3-phosphate and lactate advocates in favor of the assumption that Jen1p protein pore would be of greater geometric similarity to the less wide channel of GlpT as compared to the one of LacY. On the basis of this hypothesis and the higher accordance of the GlpT-based model with mutagenesis data, all subsequent docking calculations were performed on the GlpT-based model. The conformational space of the protein-ligand complex was extensively explored by the use of a mixed sampling protocol implementing stochastic Monte Carlo and low frequency mode conformational searches (Kolossváry *et al.*, 1996). The method has proven highly efficient in sampling molecular systems and although inferior to MD simulations from the physical point of view concerning intermediate search steps, it is considered as a robust technique. Simulations performed on the basis of the aforementioned extensive sampling protocol afforded a fair amount of structural as well as dynamic insight regarding factors that govern or influence the translocation of the various substrates across the pore of the transporter. All molecular simulations were performed using the AMBER* forcefield and the GB/SA implicit water model as they are implemented in MacroModel v.9 software (Mohamadi *et al.*, 1990).

References

Abramson J., Smirnova I., Kasho V., Verner G., Kaback R.H., Iwata S. (2003) Structure and Mechanism of the Lactose Permease of *Escherichia coli*. *Science* **301**:610-615.

Andrade R.P., Kötter P., Entian K.D., Casal M. (2005) Multiple transcripts regulate glucose-triggered mRNA decay of the lactate transporter JEN1 from *Saccharomyces cerevisiae*. *Biochem Biophys Res Commun.* **332**:254-262.

Boles E., de Jong-Gubbels P., Pronk J.T. (1998) Identification and characterization of MAE1, the *Saccharomyces cerevisiae* structural gene encoding mitochondrial malic enzyme. *J Bacteriol.* **180**:2875-82.

Casal M., Paiva S., Andrade R.P., Gancedo C., Leão C. (1999) The lactate-proton symport of *Saccharomyces cerevisiae* is encoded by *JEN1*. *J Bacteriol* **181**:2620-2623.

Casal M., Paiva S., Queirós O., Soares-Silva I. (2008) Transport of carboxylic acids in yeasts. *FEMS Microbiology Reviews.* **32**: 974–994

Cunningham P., Afzal-Ahmed I., Naftalin R. (2006) Docking studies show that D-glucose and quercetin slide through the transporter GLUT1. *J.Biol.Chem.* **281**:5797-5803.

Dang S., Sun L., Huang Y., Lu F., Liu Y., Gong H., Wang J., Yan N. (2010) Structure of a fucose transporter in an outward-open conformation. *Nature* **467**:734-738.

Ganapathy V., Thangaraju M., Gopal E., Martin P.M., Itagaki S., Miyauchi S., Prasad P.D. (2008) Sodium-coupled monocarboxylate transporters in normal tissues and in cancer. *AAPS J.* **10**:193-9.

Guan L., Kaback H.R. (2006) Lessons from lactose permease. *Annu Rev Biophys Biomol Struct.* **35**:67-91.

Huang Y., Lemieux M.J., Song J., Auer M., Wang D.N. (2003) Structure and mechanism of the glycerol-3-phosphate transporter from *Escherichia coli*. *Science* **301**:616-620.

Kaback H.R., Smirnova I., Kasho V., Nie Y., Zhou Y. (2011) The alternating access transport mechanism in LacY. *J Membr Biol.* **239**:85-93.

Kolossváry I., Guida C.W. (1996) Low Mode Search. An Efficient, Automated Computational Method for Conformational Analysis: Application to Cyclic and Acyclic Alkanes and Cyclic Peptides. *J.Am.Chem.Soc.* **118**:5011-5019.

Kosti V., Papageorgiou I., Diallinas G. (2010) Dynamic elements at both cytoplasmically and extracellularly facing sides of the UapA transporter selectively control the accessibility of substrates to their translocation pathway. *J Mol Biol.* **397**:1132-43.

Kowalczyk L., Ratera M., Paladino A., Bartoccioni P., Errasti-Murugarren E., Valencia E., Portella G., Bial S., Zorzano A., Fita I., Orozco M., Carpena X., Vázquez-Ibar J.L., Palacín M. (2011) Molecular basis of substrate-induced permeation by an amino acid antiporter. *Proc Natl Acad Sci U S A.* **108**:3935-40.

Law C.J., Maloney P.C., Wang D.N. (2008) Ins and outs of major facilitator superfamily antiporters. *Annu Rev Microbiol.* **62**:289-305.

Lodi T., Diffels J., Goffeau A., Baret P.V. (2007) Evolution of the carboxylate Jen transporters in fungi. *FEMS Yeast Res.* **7**:646-656.

Lodi T., Fontanesi F., Ferrero I., Donnini C. (2004) Carboxylic acids permeases in yeast: two genes in *Kluyveromyces lactis*. *Gene* **339**: 111-119.

Manolescu A.R., Augustin R., Moley K., Cheeseman C. (2007) A highly conserved hydrophobic motif in the exofacial vestibule of fructose transporting SLC2A proteins acts as a critical determinant of their substrate selectivity. *Mol Membr Biol.* **24**:455-463.

McDermott J.R., Rosen B.P., Liu Z. (2010) Jen1p: A High Affinity Selenite Transporter in Yeast. *Mol. Biol. Cell* **21**:3934-41.

Merezhinskaya N., Fishbein W.N. (2009) Monocarboxylate transporters: past, present, and future. *Histol Histopathol.* **24**:243-64.

Mirza O., Guan L., Verner G., Iwata S., Kaback H.R. (2006) Structural evidence for induced fit and a mechanism for sugar/H^+ symport in LacY. *EMBO J.* **25**:1177-1183.

Mohamadi F., Richard N.G.J., Guida W.C., Liskamp R., Lipton M., Caufield C., Chang G., Hendrickson T., Still W.C. (1990) MacroModel-an Integrated Software System for Modeling Organic and Bioorganic Molecules Using Molecular Mechanics. *J.Comput.Chem.* **11**:440-467.

Naula C., Logan M.F., Wong E.P., Barrett P.M., Burchmore R.J. (2010) A glucose transporter can mediate ribose uptake. Definition of residues that confer substrate specificity in a sugar transporter. *J.Biol.Chem.* **285**:29721-29728.

Newstead S., Drew D., Cameron A.D., Postis V.L., Xia X., Fowler P.W., Ingram J.C., Carpenter E.P., Sansom M.S., McPherson M.J., Baldwin S.A., Iwata S. (2011) Crystal structure of a prokaryotic homologue of the mammalian oligopeptide-proton symporters, PepT1 and PepT2. *EMBO J.* **30**:417-26.

Paiva S., Devaux F., Barbosa S., Jacq C., Casal M. (2004) Ady2p is essential for the acetate permease activity in the yeast *Saccharomyces cerevisiae*. *Yeast* **21**:201-210.

Paiva S., Vieira N., Nondier I., Haguenauer-Tsapis R., Casal M., Urban-Grimal D. (2009) Glucose-induced ubiquitylation and endocytosis of the yeast Jen1 transporter: role of lysine 63-linked ubiquitin chains. *J Biol Chem.* **284**:19228-19236.

Sali A., Potterton L., Yuan F., van Vlijmen H., Karplus M. (1995) Evaluation of comparative protein modelling by MODELLER. *Proteins* **23**:318-326.

Soares-Silva I., Paiva S., Diallinas G., Casal M. (2007) The conserved sequence NXX[S/T]HX[S/T]QDXXXT of the lactate/pyruvate:H+ symporter subfamily defines the function of the substrate translocation pathway. *Mol Membr Biol.* **24**:464-474.

Soares-Silva I., Paiva S., Kötter P., Entian K.D., Casal M. (2004) The disruption of JEN1 from *Candida albicans* impairs the transport of lactate. *Mol Membr Biol.* **21**:403-411.

Soares-Silva I., Schuller D., Andrade R.P., Baltazar F., Cássio F., Casal M. (2003) Functional expression of the lactate permease Jen1p of *Saccharomyces cerevisiae* in *Pichia pastoris*. *Biochem J* **376**:781-787.

Vieira N., Casal M., Johansson B., MacCallum D.M., Brown A.J., Paiva S. (2010) Functional specialization and differential regulation of short-chain carboxylic acid transporters in the pathogen *Candida albicans*. *Mol Microbiol.* **75**:1337-1354.

Acknowledgments

We thank Vasso Kosti for help in model construction with FucP and Pet1. ISS (SFRH/BPD/22976/2005) and JP (SFRH/BD/61530/2009) received fellowships from the Portuguese government through POPH and FSE. GD was supported by the University of Athens during his sabbatical at Universidade do Minho.

Table 1 – Relative capacity (%) of ^{14}C-lactic acid uptake in the presence of non-labelled carboxylic acids, at the indicated concentration, acting as competitors for the transport of lactate in mutants having a measurable transport capacity (>25%).

	% ^{14}C-Lactic acid uptake							
Inhibitor / Mutant	Lactic 0.3mM		Pyruvic 0.7mM		Succinic 60mM		Malic 60mM	
WT Jen1	29.9	± 0.0	39.4	± 0.0	100.0	± 0.0	100.0	± 0.0
S266A	30.8	± 4.1	13.2	± 1.1	66.1	± 0.7	61.5	± 5.1
F270G	29.9	± 0.1	19.3	± 0.0	**24.3**	**± 10.7**	**37.4**	**± 4.3**
F270Y	39.0	± 0.4	63.4	± 8.6	63.6	± 3.1	68.3	± 4.1
F270A	71.2	± 15.6	20.5	± 5.6	**34.9**	**± 10.1**	**48.9**	**± 13.4**
S271Q	74.5	± 31.2	42.2	± 15.8	107.9	± 17.6	112.6	± 2.4
S271E	54.9	± 21.9	34.1	± 16.7	99.3	± 13.6	91.9	± 14.4
F270QS271Q	32.0	± 0.8	26.7	± 0.0	**50.6**	**± 1.2**	**44.8**	**± 2.6**
A272G	**18.9**	**± 0.5**	**9.9**	**± 0.2**	61.5	± 2.6	55.8	± 4.2
Y284Q	27.3	± 1.3	18.8	± 0.2	86.7	± 5.8	83.7	± 5.9
Y284T	31.8	± 6.0	24.1	± 2.4	104.8	± 17.7	95.1	± 5.0
Q498N	49.9	± 17.7	28.9	± 10.9	99.8	± 14.7	110.5	± 8.5
Q498A	32.5	± 0.2	14.7	± 1.3	60.1	± 8.5	67.6	± 0.2
N501D	**110.4**	**± 0.1**	**78.1**	**± 19.7**	117.7	± 11.3	127.3	± 10.7

The data shown are mean values, in percentage, of at least 3 independent experiments, with three replicas, and the respective standard deviation preceded by ±.

Table 2 – Kinetic parameters of ^{14}C-lactic acid transport (maximum velocity, V_{max}, and affinity constant, K_m) for some mutants, compared to the wild-type protein.

	Lactic acid transport kinetic parameters	
Mutant	V_{max} (nmol.s^{-1}.mg dry wt^{-1})	K_m (mM)
WT Jen1	0.16 ± 0.02	0.68 ± 0.30
S266A	0.08 ± 0.01	0.40 ± 0.13
F270G	0.15 ± 0.01	0.97 ± 0.16
F270QS271Q	0.22 ± 0.01	0.21 ± 0.05
A272G	0.24 ± 0.02	0.21 ± 0.07
Q498A	0.18 ± 0.03	1.61 ± 0.58
N501D	0.14 ± 0.01	1.42 ± 0.33

The transport kinetics best fitting the experimental initial uptake rates and the kinetic parameters were determined by a computer-assisted nonlinear regression analysis (GraphPAD Software, San Diego, CA, USA). The data shown are mean values of at least 3 independent experiments, with three replicas, and the respective standard deviation preceded by ±.

Table 3 – Inhibition constant (K_i) of ^{14}C-lactic acid uptake for succinic and malic acids of the mutants able to grow in dicarboxylates.

	K_i (mM)	
Inhibitor / Mutant	Succinic	Malic
F270G	1.92	3.38
F270QS271Q	1.85	28.07
Q498A	29.83	33.46

The kinetic parameters were determined by a computer-assisted nonlinear regression analysis (GraphPAD Software, San Diego, CA, USA). The data shown are mean values of at least 3 independent experiments, with three replicas.

Figure legends

Fig. 1 Multiple sequence alignment of TMS-II, TMS-V and TMS-XI of Jen1 homologues. Residues mutated in this work are highlighted in black boxes. The alignment was build using the ClustalW2 bioinformatics tool. (http://www.ebi.ac.uk/Tools/clustalw2/). Sc, Kl and Ca denote *S. cerevisiae, K. lactis* and *C. albicans* permeases of known specificity for mono- (Jen1) or dicarboxylates (Jen2). MaJen1, NcJen1 and TaJen1 denote Jen1 homologues of unknown function from *Metarhizium anisopliae*, *Neurospora crassa* and *Thermoplasma acidophilum*. Accession numbers, in order of appearance, NP_012705, CAG99769, XP_716108, AAM77971, XP_962841, CAC11721, XP_717031, CAG98245. An evolutionary relationship of mono and di-carboxylate transporters can be found in Casal *et al*,, 2008.

Fig. 2 Relative % of Jen1p-mediated [^{14}C]-lactic acid transport in mutants at 30 ^{o}C. The % uptake rate of the wild-type Jen1p (WT Jen1 – *S.cerevisiae Δjen1Δady2* carrying the plasmid pDS1) is considered 100%. For wild-type and the cryosensitive mutants S271Q or S271E similar uptake measurements were also performed at 18 ^{o}C (see text).The data shown are mean values of at least 3 independent experiments and the error bars represent standard deviation.

Fig. 3 Epifluorescent microscopy of GFP-tagged version of Jen1p in a control strain and mutants (for details see Experimental procedures). In all cases, Jen1-GFP molecules label the plasma membrane.

Fig. 4 A) Growth test of control strains and mutants on glucose (2%), lactic acid (0.5%) or succinic acid (1%). All strains are isogenic (*S. cerevisiae* W303-1A *ΔJen1 ΔAdy2*) expressing from a low copy plasmid either wild-type Jen1 (WT-Jen1) or the relevant Jen1 alleles. The negative control is a strain carrying an empty vector (ΔJen1). B) Relative resistance/sensitivity of control strains and mutants on 200 µM Selenite. The relative % of Jen1 [^{14}C]-lactic acid uptake is indicated in both A and B.

Fig. 5 Overall structure of the Jen-1 model. A) A section of the transporter as viewed from the periplasmic side. Visible is the spiral rim-like network of hydrogen bonds that is formed. B) Side view of the protein. Residues that define the translocation pathway are illustrated as green spheres.

Fig. 6 Illustration of the F270-S271 residue pair location within helix V and their surrounding environment with respect to the overall Jen1 topology. F270 forms a close contact with helix VIII, at the position where a kink appears at half-length of the latter. The phenyl group of F270 demonstrates extensive packing interactions with the hydrophobic sidechains of I416 and M420, both belonging to TMS VIII. On the other side of TMS V, the polar S271 is engaged in an intrahelical hydrogen bond with the backbone carbonyl of G267. The position as well as the interaction pattern of F270 with surrounding tertiary structure elements could support the hypothesis that this specific residue holds an important role in facilitating helix packing, stabilizing tertiary structure and, ultimately, influencing the dynamics of the inward-to-outward transition of the protein, thus accounting for its functionality as a substrate specificity determinant.

Fig. 7 The stepwise translocation pathway of lactate across the Jen1p pore, as proposed by simulations performed on the lactate-transporter complex. A flexible pattern of interactions formed mainly between the substrate and the side-chain of R188 mediates the sliding movement of the former towards the cytoplasmic side of the transporter for a total length exceeding 10Å. This movement is accompanied by the reorientation of the R188 side-chain which, to this respect and according to simulations, could hold the role of a mobile anchoring point that drives the substrate translocation process through sequential attractive interactions originating by pairing the aforementioned arginine with H383, N501 or Q498.

Fig. 8 The translocation pathway followed by the substrate along the pore of Jen1p transporter, as revealed by molecular simulations. The transporter is represented by its molecular surface and lactate is depicted in a stick representation. Transmembrane helices IV and XI are partially not shown for clarity. Helices II (yellow) and VII (orange) are presented as ribbons. Extended stochastic sampling of the substrate-protein complex conformational space resulted in an ensemble of low-energy conformations, thus defining a (hypothetical/potential) track along which the transport could be carried out. This simulated translocation course of the substrate within the pore was fully consistent with the topology of the residues identified and characterized as critical by kinetics and mutagenesis experiments. The positioning of those among the critical residues that are specifically located on helices II and VII are indicated by dashed lines.

Figure 1

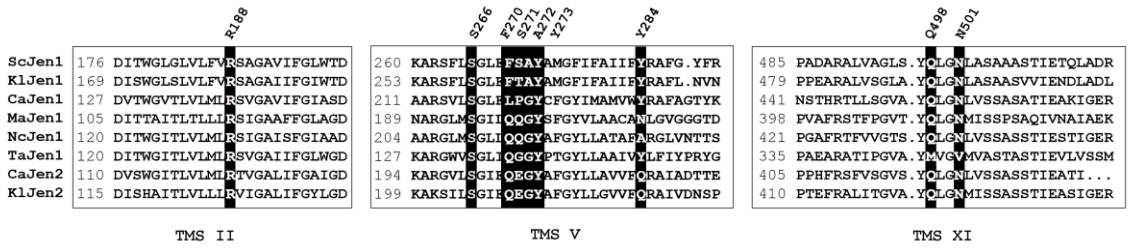
R188
S266
F270
S271
R272
Y273
Y284
Q498
N501
ScJen1 176 DITWGLGLVLFVRSAGAVIFGLWTD 260 KARSFLSGLEFSAYAMGFIFAIIFYRAFG.YFR 485 PADARALVAGLS.YQLGNLASAAASTIETQLADR
KlJen1 169 DISWGLSLVLFVRSAGAIIFGIWTD 253 KARSFLSGLEFTAYAMGFIFAIIFYRAFL.NVN 479 PPEARALVSGLA.YQLGNLASAASVVIENDLADL
CaJen1 127 DVTWGVTLVLMLRSVGAVIFGIASD 211 AARSVLSGLELPGYCFGYIMAMVWYRAFAGTYK 441 NSTHRTLLSGVA.YQLGNLVSSASATIEAKIGER
MaJen1 105 DITTAITLTLLLRSIGAAFFGLAGD 189 NARGLMSGILQQGYSFGYVLAACANLGVGGGTD 398 PVAFRSTFPGVT.YQLGNMISSPSAQIVNAIAEK
NcJen1 120 DITWGITLVLMLRSIGAISFGIAAD 204 AARGLMSGLLQQGYAFGYLLATFARGLVNTTS 421 PGAFRTFVVGTS.YQLGNLVSSASSTIESTIGER
TaJen1 120 DITWGITLVLMLRSVGAIIFGLWGD 127 KARGWVSGLLQGGYPTGYLLAAIVYLFIYPRYG 335 PAEARATIPGVA.YMVGVMVASTASTIEVLVSSM
CaJen2 110 DVSWGITLVLMLRTVGALIFGAIGD 194 KARGVLSGILQEGYAFGYLLAVVFQRAIADTTE 405 PPHFRSFVSGVS.YQLGNLVSSASSTIEATI...
KlJen2 115 DISHAITLVLLLRVIGALIFGYLGD 199 KAKSILSGILQEGYAFGYLLGVVFQRAIVDNSP 410 PTEFRALITGVA.YQLGNMISSASSTIEASIGER
TMS II
TMS V
TMS XI

Figure 2

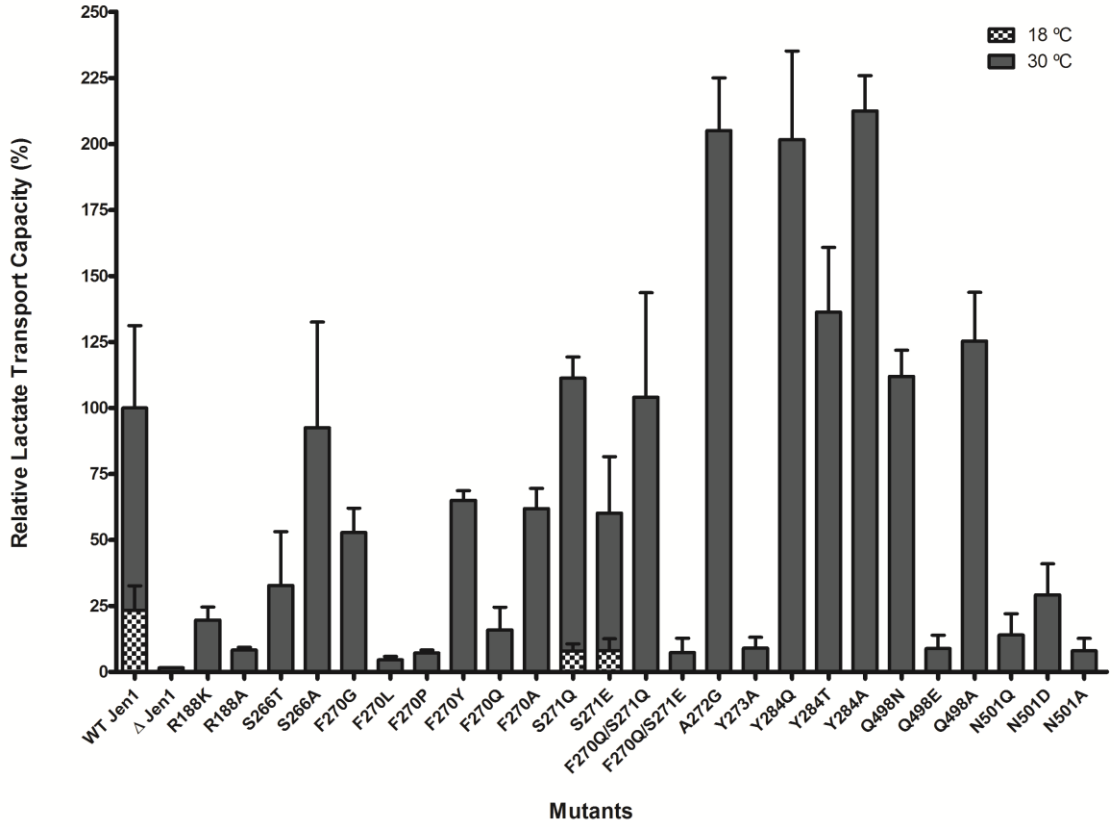
18 ℃
30 ℃
Relative Lactate Transport Capacity (%)
250
225
200
175
150
125
100
75
50
25
0
WT Jen1
Δ Jen1
R188K
R188A
S266T
S266A
F270G
F270L
F270P
F270Y
F270Q
F270A
S271Q
S271E
F270Q/S271Q
F270Q/S271E
A272G
Y273A
Y284Q
Y284T
Y284A
Q498N
Q498E
Q498A
N501Q
N501D
N501A
Mutants

Figure 3

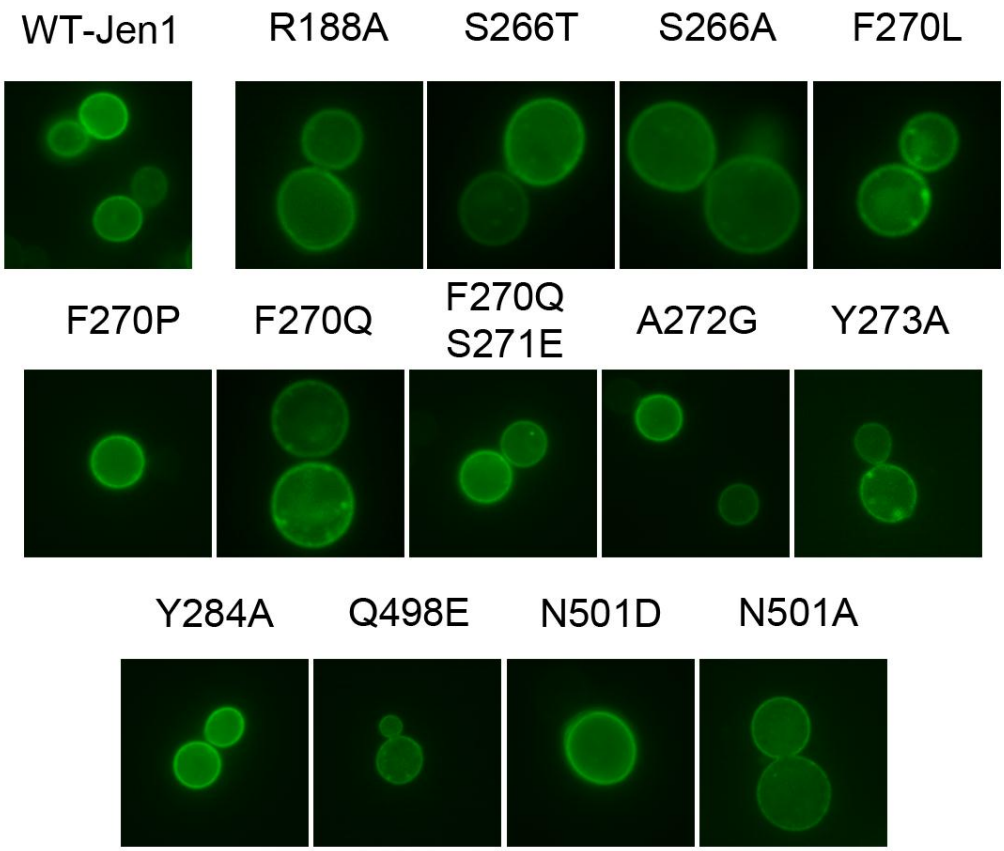
WT-Jen1
R188A
S266T
S266A
F270L
F270P
F270Q
F270Q
S271E
A272G
Y273A
Y284A
Q498E
N501D
N501A

Figure 4

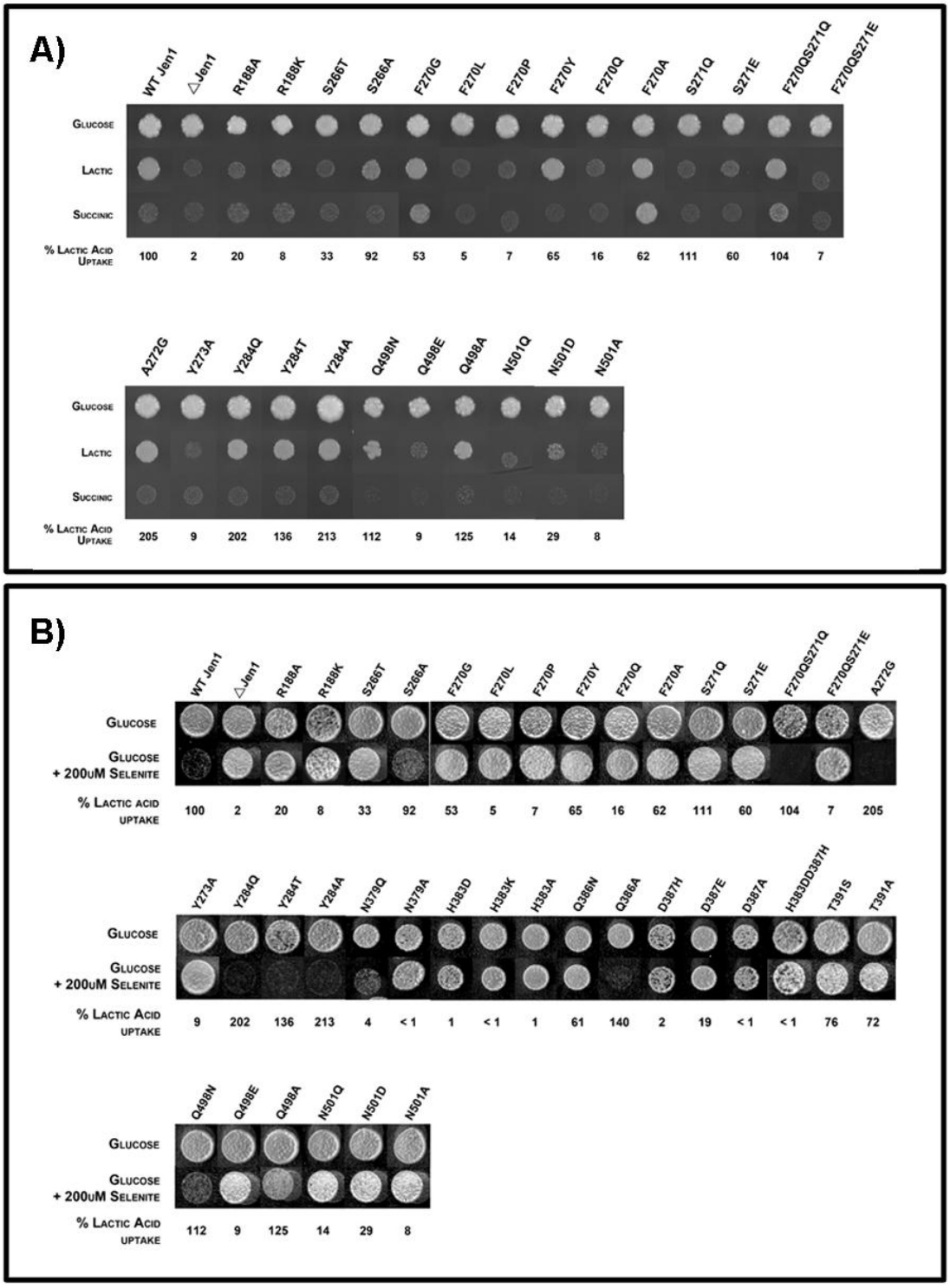
A)
WT Jen1
△Jen1
R188A
R188K
S266T
S266A
F270G
F270L
F270P
F270Y
F270Q
F270A
S271Q
S271E
F270QS271Q
F270QS271E
Glucose
Lactic
Succinic
% Lactic Acid Uptake
100 2 20 8 33 92 53 5 7 65 16 62 111 60 104 7
A272G
Y273A
Y284Q
Y284T
Y284A
Q498N
Q498E
Q498A
N501Q
N501D
N501A
Glucose
Lactic
Succinic
% Lactic Acid Uptake
205 9 202 136 213 112 9 125 14 29 8
B)
WT Jen1
△Jen1
R188A
R188K
S266T
S266A
F270G
F270L
F270P
F270Y
F270Q
F270A
S271Q
S271E
F270QS271Q
F270QS271E
A272G
Glucose
Glucose + 200uM Selenite
% Lactic acid uptake
100 2 20 8 33 92 53 5 7 65 16 62 111 60 104 7 205
Y273A
Y284Q
Y284T
Y284A
N379Q
N379A
H383D
H383K
H383A
Q386N
Q386A
D387H
D387E
D387A
H383DD387H
T391S
T391A
Glucose
Glucose + 200uM Selenite
% Lactic Acid uptake
9 202 136 213 4 < 1 1 < 1 1 61 140 2 19 < 1 < 1 76 72
Q498N
Q498E
Q498A
N501Q
N501D
N501A
Glucose
Glucose + 200uM Selenite
% Lactic Acid uptake
112 9 125 14 29 8

Figure 5

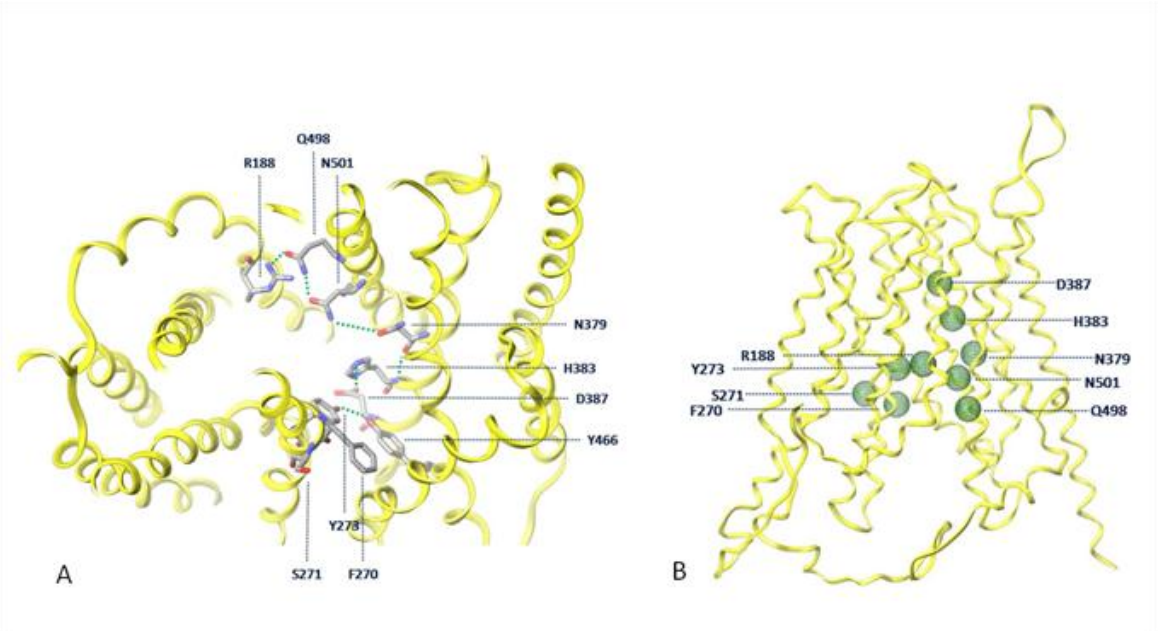
Q498
R188
N501
N379
H383
D387
Y466
Y273
S271
F270
A
D387
H383
R188
N379
Y273
N501
S271
F270
Q498
B

Figure 6

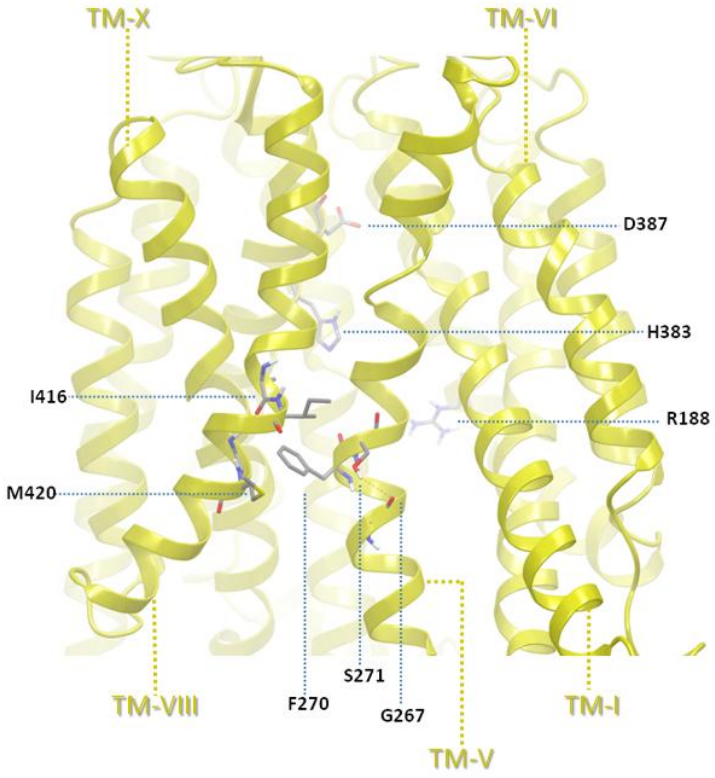
TM-X
TM-VI
D387
H383
I416
R188
M420
S271
TM-VIII
F270
G267
TM-I
TM-V

Figure 7

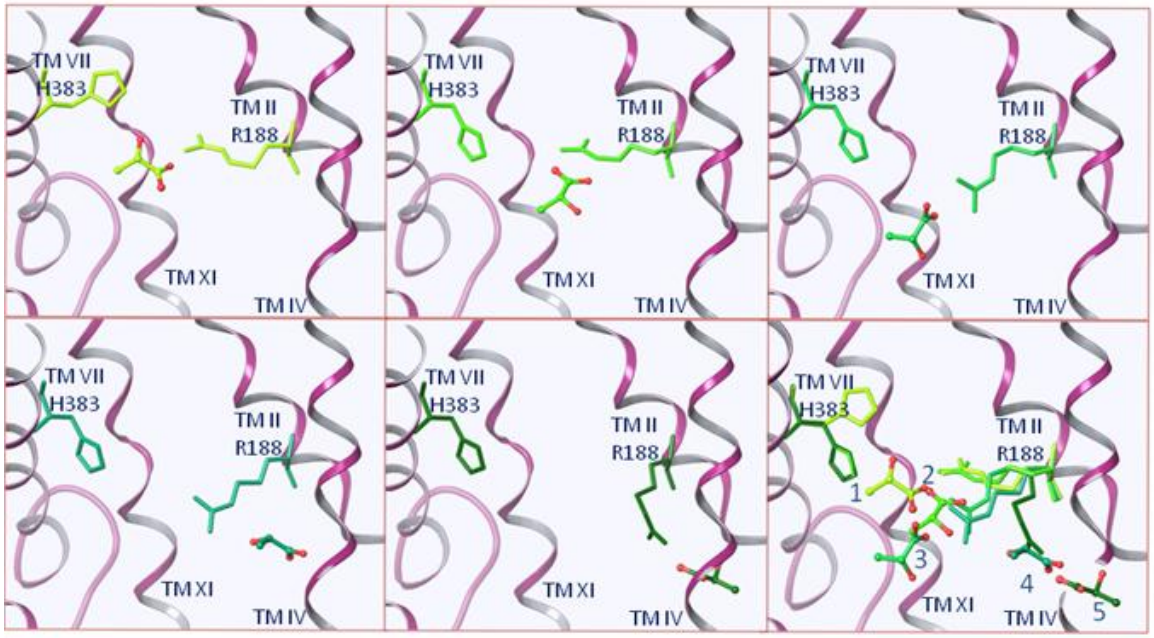

Figure 8